nature chemical engineering

Article

https://doi.org/10.1038/s44286-023-00006-0

Carbon–carbon bond cleavage for a lignin refinery

Received: 13 April 2023

Accepted: 22 November 2023

Published online: 11 January 2024

Check for updates

Zhicheng Luo[1,2,5] ✉, Chong Liu[3,5], Alexandra Radu[1,5], Davey F. de Waard[1], Yun Wang[2], Jean T. Behaghel de Bueren[4], Panos D. Kouris[1], Michael D. Boot[1], Jun Xiao[2], Huiyan Zhang[2], Rui Xiao[2] ✉, Jeremy S. Luterbacher[4] & Emiel J. M. Hensen[1] ✉

Carbon–carbon bonds, ubiquitous in lignin, limit monomer yields from current depolymerization strategies, which mainly target C–O bonds. Selective cleavage of the inherently inert σ-type C–C bonds without pre-functionalization remains challenging. Here we report the breaking of C–C bonds in lignin obtained upon initial disruption of labile C–O bonds, achieving monocyclic hydrocarbon yields up to an order of magnitude higher than previously reported. The use of a Pt (de)hydrogenation function leads to olefinic groups close to recalcitrant C–C bonds, which can undergo β-scission over zeolitic Brønsted acid sites. After confirming that this approach can selectively cleave common C–C linkages (5–5′, β–1′, β–5′ and β–β′) in lignin skeletons, we demonstrate its utility in the valorization of various representative lignins. A techno-economic analysis shows the promise of our method for producing gasoline- and jet-range cycloalkanes and aromatics, while a life-cycle assessment confirms its potential for CO_2-neutral fuel production.

Lignocellulosic biomass, the most abundant renewable feedstock on Earth, can replace fossil resources to produce fuels, chemicals and materials[1–3]. It consists of cellulose (35%–50%), hemicellulose (20%–35%) and lignin (10%–25%)[4]. Traditionally, lignin is burned to generate power, mainly in the pulp and paper industry, where the cellulose part of biomass is the main product[5]. The advent of second-generation biorefineries will generate more lignin waste, which needs to be converted to valuable products to render these operations economically viable[6].

Depolymerization of lignin into fragments with lower molecular mass suitable for downstream processing is one of the most promising approaches to obtaining value-added products from lignin side streams[6–9]. Lignin is randomly linked by C–C bonds (5–5′, β–5′, β–1′ and β–β′) and C–O bonds (β–O–4′, α–O–4′ and 4–O–5′) with respective contents of 20–40% and 60–80% in lignocellulosic biomass (Fig. 1a)[10]. Cleaving the relatively labile β–O–4′ bonds is the primary depolymerization strategy for obtaining monomers[11]. The 'maximum monomer' yield based on cleaving these bonds can be approximated as the square of the fraction of β–O–4′ bonds[12]. For lignin with a relatively high β–O–4′ content of 70%, the maximum monomer yield will be 49%.

Extracting uncondensed lignin with a high β–O–4′ content during biomass fractionation (Fig. 1a) can facilitate the subsequent production of lignin monomers[13]. Biomass fractionation in paper and pulp manufacture ('harsh' fractionation in Fig. 1a) involves using mineral acids or bases at relatively high temperatures to remove lignin and hemicellulose from the lignocellulosic matrix[14]. Under such severe conditions, lignin undergoes irreversible condensation, where the C–O bonds break and new recalcitrant C–C bonds form, yielding a

[1]Laboratory of Inorganic Materials and Catalysis, Department of Chemical Engineering and Chemistry, Eindhoven University of Technology, Eindhoven, the Netherlands. [2]MOE Key Laboratory of Energy Thermal Conversion & Control, School of Energy and Environment, Southeast University, Nanjing, China. [3]State Key Laboratory of Structural Chemistry, Fujian Institute of Research on the Structure of Matter, Chinese Academy of Sciences, Fuzhou, Fujian, China. [4]Laboratory of Sustainable and Catalytic Processing, Institute of Chemical Sciences and Engineering, Ecole Polytechnique Fédérale de Lausanne, Lausanne, Switzerland. [5]These authors contributed equally: Zhicheng Luo, Chong Liu, Alexandra Radu. ✉e-mail: zluo@seu.edu.cn; ruixiao@seu.edu.cn; e.j.m.hensen@tue.nl

https://doi.org/10.1038/s44286-023-00006-0

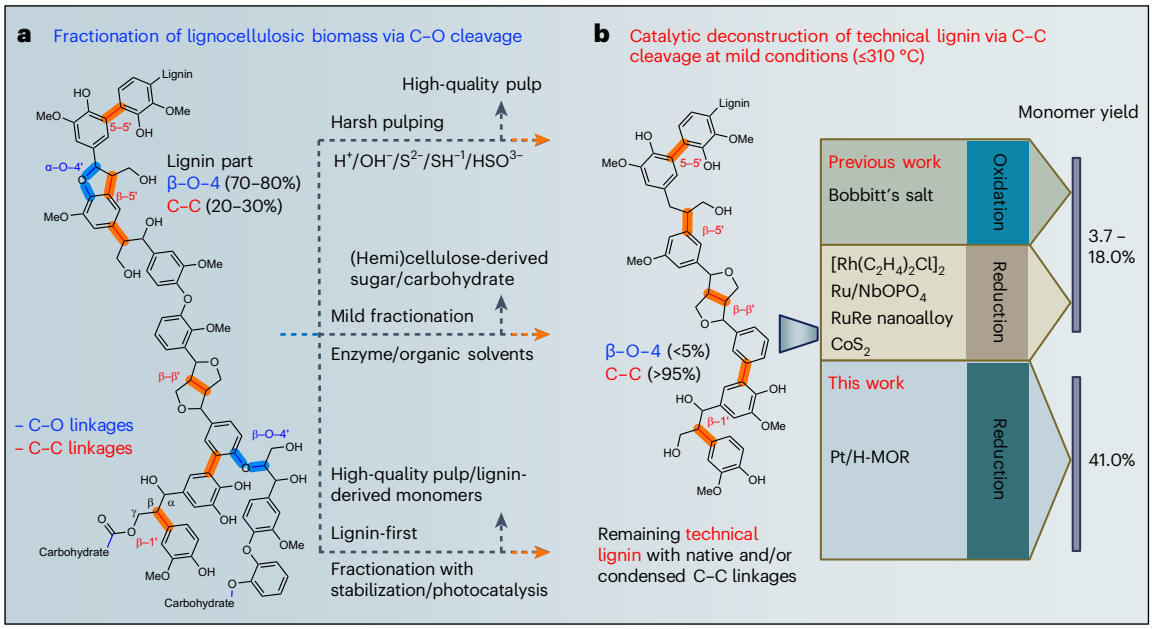

Fig. 1 | Valorization of lignocellulosic biomass. a, State-of-the-art approaches for the fractionation of lignocellulosic biomass via C–O cleavage. The C–C and C–O bonds in lignin are highlighted in red and blue, respectively. **b**, Current and proposed catalytic approaches for the deconstruction of technical lignin via C–C cleavage under mild conditions (≤310 °C).

highly condensed lignin. Mild fractionation, including ammonia-based fractionation[15], ionic liquid-assisted fractionation[16], γ-valerolactone-assisted hydrolysis[17] and organosolv approaches[18], results in more reactive (that is, less condensed) lignins, in which the disruption of C–O bonds and the concurrent formation of reactive intermediates is diminished. The drawback of mild fractionation is that the yield of isolated lignin with a relatively high β–O–4′ content is usually low. Increasing the extent of delignification requires harsher conditions, which reduces the β–O–4′ content in the extracted lignin. This trade-off was demonstrated in a recent study covering 27 types of lignin, where conservation of high β–O–4′ content was accompanied by a low yield of isolated lignin[19]. The lignin-first strategy, which has emerged recently, focuses on separating lignin from the lignocellulosic matrix, resulting in a lignin oil and a solid carbohydrate pulp[20,21]. A promising lignin-first approach comprises reductive catalytic fractionation (RCF), where lignin–carbohydrate bonds are broken by hydrogenolysis. At the same time, the released lignin fragments are further hydrogenated to a lignin oil with a yield close to the maximum monomer yield based on the β–O–4′ content[22]. However, this lignin-first strategy is also hampered by the inability to cleave C–C bonds, which leaves a highly condensed, high-molecular-weight technical lignin residue with many C–C linkages.

The C–C bonds in technical lignin can be categorized into aryl–aryl (5–5′), aryl–alkyl (β–5′) and alkyl–alkyl (β–1′ and β–β′). Their high dissociation energies in the 226–494 kJ mol^{-1} range hamper the optimal valorization of this important renewable resource[23,24]. To extract more monomers from technical lignin, approaches that can cleave the recalcitrant C–C bonds are needed. Samec and colleagues reported the oxidative cleavage of aryl–alkyl and alkyl–alkyl linkages in lignin with the formation of 2,6-dimethoxybenzoquinone in a yield of 18%, corresponding to a total monomer yield of 132% relative to the maximum monomer yield (Fig. 1b)[25]. However, the oxidation approach only cleaved C–C bonds in lignin fragments containing free phenolic groups but not aryl–aryl bonds. Another drawback is that the stoichiometric oxidant must be regenerated.

It would be highly desirable if the scission of various C–C bonds could be achieved by one-pot reductive chemistry. The main challenge is to break these C–C bonds selectively. Typically, the high reaction temperatures (>310 °C) required to break C–C bonds lead to extensive cracking and low yields of desirable ring products[26]. Compared to cracking, catalytic hydrogenolysis at milder conditions (≤310 °C) can be carried out with higher selectivity[27–32]. Dong and colleagues used a rhodium-based catalyst to break the aryl–aryl bond in 2,2′-biphenols, which are abundant in lignin (Fig. 1b)[28], and unstrained aryl–alkyl bonds in phenolic resins[29]. However, this method cannot break alkyl–alkyl bonds. Concerns for the practical implementation of this innovative approach are that the catalyst requires the absence of water and the use of substantial amounts of phosphinites as a modifying group. Under relatively mild reaction conditions of 310 °C and 5 bar H_2, a Ru/$NbOPO_4$ catalyst was reported to cleave C–C bonds in lignin selectively, resulting in the formation of monocyclic hydrocarbons in a yield of 8.0–9.9% (Fig. 1b)[32]. The total monomer yield achieved was 124–153% relative to the maximum monomer yield. Despite the high selectivity for cleaving aryl–aryl and aryl–alkyl bonds, the catalyst displayed no activity for breaking alkyl–alkyl bonds, which limits the monomer yield. Thus, there remains a need for a hydrogenation approach to selectively disrupt all three types of C–C linkage in lignin under mild reaction conditions.

In this Article we report a mild and reductive catalytic approach employing a bifunctional Pt/H-MOR catalyst to depolymerize technical lignin to obtain monomers in a 2–11-times higher yield than reported in the literature. The utility of this approach is illustrated by selective cleavage of aryl–aryl, aryl–alkyl and alkyl–alkyl in seven different lignins at a relatively low temperature of 300 °C. Mechanistic studies show that the Brønsted acid sites in H-MOR can directly cleave aryl–alkyl bonds. Pt/H-MOR catalyzes the cleavage of aryl–aryl and alkyl–alkyl compounds via bifunctional catalysis, where Pt hydrogenates aryl moieties and introduces double bonds in alkyl ones, followed by acid-catalyzed β-scission. This approach substantially improves the monomer yield, with the best results constituting a 58–409% increase over the conventional maximum monomer yield obtainable for the investigated lignins.

Results and discussion

For catalyst screening, we used a model lignin dimer (2,2′-biphenol, **1**), representative of the 5–5′-linked units (C–C bonds) ubiquitous in lignin and with the highest bond dissociation energy in the 481–494 kJ mol^{-1} range[24]. The reductive cleavage of C–C bonds in **1** was evaluated at a

https://doi.org/10.1038/s44286-023-00006-0

a

Entry	Feedstock	Catalyst	Yield (C%)					Conversion (C%)
			Monomers		Dimers			
			13	**14**	**10**	**11**	**7**	
1[a]	**1**	None	0	0	0	0	0	0
2[a]	**1**	Pt/SiO_2	0	0	92.3	7.7	0	100
3[a]	**1**	Pt/Nb_2O_5	0	0	94.7	5.3	0	100
4[a]	**1**	Pt/TiO_2	0	0	47.4	2.7	0	100
5[a]	**1**	H-MOR	0	0	0	0	100	100
6[a]	**1**	Pt/SiO_2 + H-MOR	5.0	3.0	57.4	9.7	0	100
7[a]	**1**	Pt/H-MOR	70.3	16.0	4.2	2.0	1.2	100
8[a]	**1**	Pt/Na-MOR	0	0	35.3	2.8	61.9	100
9[a]	**1**	Pt/SiO_2-Al_2O_3	1.2	0.9	95.0	2.9	0	100
10[a]	None	Pt/H -MOR	0	0	0	0	0	0

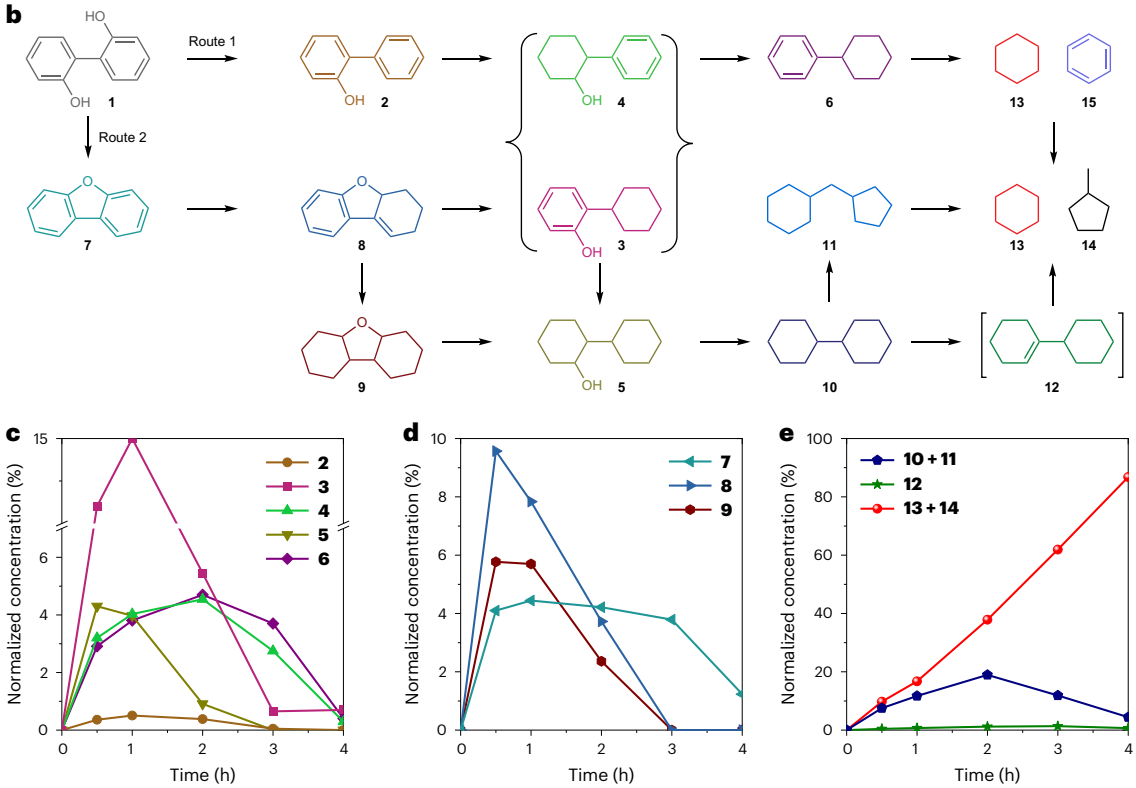

Fig. 2 | Reductive C–C cleavage of 2,2′-biphenol (1). a, Reductive cleavage of **1** using various catalysts. Conversion and yield are defined in Supplementary Section 1.3. **b**, Proposed reaction pathways for the conversion of **1** over Pt/H-MOR. **c**–**e**, Time-course reaction profiles for Pt/H-MOR-catalyzed depolymerization of **1** to monomers, showing the selective cleavage of C–C bonds for **2**–**6** (**c**), **7**–**9** (**d**) and **10**–**14** (**e**). [a]Reaction conditions: **1** (20 mmol l^{-1}), 50 mg catalyst, 40 ml *n*-pentane, 260 °C, 4 h and 40 bar H_2.

temperature of 260 °C and an H_2 pressure of 40 bar using *n*-pentane as the solvent. Figure 2a shows the results for the different catalysts explored. The most important physicochemical properties of these catalysts are reported in Extended Data Table 1 and Supplementary Fig. 1. Without a catalyst, **1** was not converted under these conditions. In the presence of Pt/SiO_2, **1** was completely converted to mainly bicyclohexyl (**10**) and a small amount of cyclopentylmethylcyclohexane (**11**). With H-MOR as the catalyst, **1** was quantitatively dehydrated to dibenzofuran (**7**). By combining Pt/SiO_2 and H-MOR, monomers such as cyclohexane (**13**) and methylcyclopentane (**14**) were obtained with a total yield of 8.0%. The monomer yield from the conversion of **1** improved to 86.3% when Pt/H-MOR was used instead of a physical mixture of Pt/SiO_2 and H-MOR. Its non-acidic counterpart, Pt/Na-MOR, did not afford monomers. The low activity obtained with Pt/SiO_2–Al_2O_3 can be attributed to the low acidity of amorphous silica–alumina. Other common Pt/acid–base catalysts, such as Pt/Nb_2O_5 and Pt/TiO_2, did not result in monomers either. The preference for Pt/H-MOR was further compared by varying the Brønsted acid support and the metal (Supplementary Note 1). It was verified that the *n*-pentane solvent was not converted to monomers by carrying out the experiment without **1** with Pt/H-MOR (Supplementary Figs. 2 and 3 and Supplementary Table 2). A recent study reported a Pt/CDC–SiC (carbide-derived carbon–SiC composite) catalyst that achieved a monomer yield of 49.3 wt% by cleaving the C–C bond in **1** assisted by microwave irradiation[30].

https://doi.org/10.1038/s44286-023-00006-0

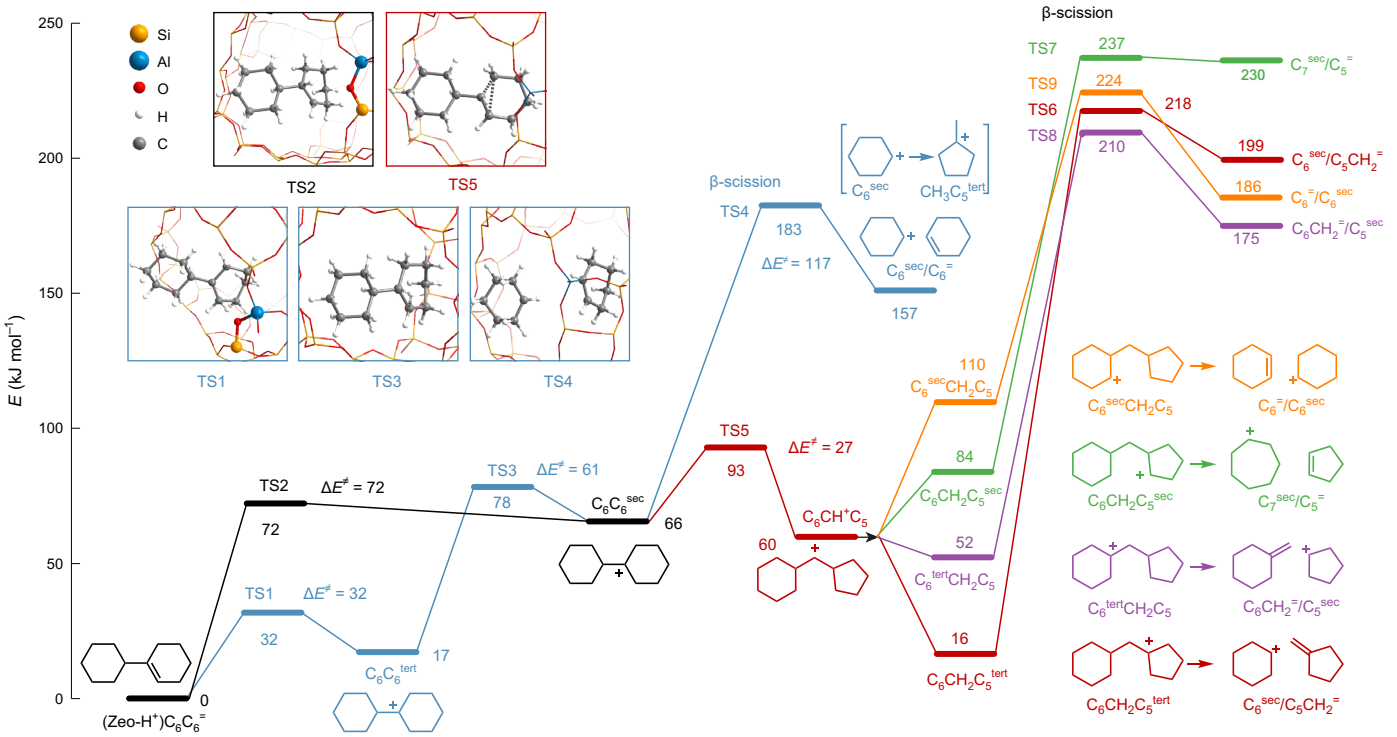

Fig. 3 | DFT study of the reaction mechanism of C–C bond cleavage. Potential energy diagram for proposed reaction pathways of C–C bond cleavage in **12** over H-FAU zeolite. Energies are given with respect to the adsorption state of [(Zeo–H$^+$)$C_6C_6^=$]. The most important transition states are shown top left.

Our results demonstrate an improved total monomer yield of 86.3%, outperforming the previously reported highest yield of 80.7% using a RuRe alloy catalyst[31].

Figure 2b proposes the main reaction pathways during conversion of **1** over Pt/H-MOR, including the major reaction intermediates and products (Supplementary Fig. 4): 2-hydroxybiphenyl (**2**), 2-cyclohexylphenol (**3**), 2-phenylcyclohexanol (**4**), 2-cyclohexylcyclohexanol (**5**), cyclohexylbenzene (**6**), dibenzofuran (**7**), tetrahydrodibenzofuran (**8**), dodecahydrodibenzofuran (**9**), bicyclohexyl (**10**), cyclopentylmethylcyclohexane (**11**), 3-cyclohexylcyclohexene (**12**), cyclohexane (**13**) and methylcyclopentane (**14**). These pathways are based on the time-course profiles displayed in Fig. 2c–e, and the rates of the individual reaction steps are provided in Supplementary Table 3. Following an earlier study on the hydrodeoxygenation of guaiacol[33], we report here pseudo-first-order reaction rate constants to compare the reactivities of the different compounds. Figure 2c shows that **2** is a reaction intermediate obtained by the removal of one of the hydroxyl groups in **1** over Pt. **2** is then partially hydrogenated to **3** and **4** with a reaction rate of 14.6 mmol l^{-1} h^{-1}. **3** and **4** are hydrogenated to **5**, and removal of the other hydroxyl group yields **6**. Removal of the second hydroxyl group from **5** results in **10** and its isomer **11**. Figure 2d demonstrates that **7** is another reaction intermediate obtained from **1** by dehydration over H-MOR with a reaction rate of 15.1 mmol l^{-1} h^{-1}. Intermediate **7** can be hydrogenated to **8** and **9** with an overall hydrogenation rate of 23.9 mmol l^{-1} h^{-1}. Intermediates **8** and **9** can then be converted to **6** and **10** + **11**. C–C bond cleavage in **10** results in the main monomeric products **13** and **14** with an overall reaction rate of 2.6 mol l^{-1} h^{-1} (Fig. 2e). Relevant to cleavage of the alkyl–alkyl moiety in **10** is the observation of compound **12** with a C=C bond that allows C–C bond cleavage via β-scission over H-MOR. Note that **10** was not converted by Pt catalysts supported on SiO_2, Nb_2O_5, Al_2O_3 and TiO_2 containing Lewis acid and basic sites (Supplementary Table 4). This demonstrates that the Brønsted acid sites in H-MOR are indispensable for alkyl–alkyl cleavage. The cracking of **6** should also be considered as a pathway to the monocyclic products. The contributions of cracking via intermediates **10** and **6** were then investigated by studying their conversions in separate experiments.

The conversion of bicyclohexyl (**10**) over Pt/H-MOR resulted in **13** and **14** as monocyclic products (Supplementary Fig. 5a), confirming that alkyl–alkyl bonds can be cracked by our approach. Unlike for **1**, the conversion of **10** led to heavier products (Supplementary Note 2). Cracking was also achieved with a physical mixture of Pt/SiO_2 and H-MOR (Supplementary Fig. 5b), but not with Pt/SiO_2 or H-MOR (Supplementary Table 4). This confirms the bifunctional nature of the cleavage of **10**[34]. Different from the conversion of **1**, cyclohexylcyclohexene (**12**) was not observed during the conversion of **10**. However, by lowering the hydrogen pressure to 5 bar, this intermediate was observed (Supplementary Fig. 6). A specific aspect of bifunctional hydrocracking of hydrocarbons is that the distance between the two catalytic functions affects the overall rate[35]. In the present work, this is evident from the substantially higher C–C cleavage rate of **10** for Pt/H-MOR (2.6 mmol l^{-1} h^{-1}) than for the physical mixture of Pt/SiO_2 and H-MOR (0.8 mmol l^{-1} h^{-1}), suggesting that slow diffusion of unsaturated intermediates between Pt and acid sites suppresses the overall rate.

We then studied C–C cleavage in the unsaturated intermediate cyclohexylbenzene (**6**) observed during the conversion of **1** over H-MOR without hydrogen (Supplementary Fig. 7a). Products **13**, **14** and benzene (**15**) were formed as the main monocyclic products, confirming that the aryl–alkyl moiety in **6** can be directly cleaved by H-MOR. The observation of small amounts of cyclohexene (**16**) and 1-methylcyclopentene (**17**) suggests that dehydrogenation of the cyclohexyl ring in **6** is a possible pathway. The observation of H_2 in the gas phase during this experiment confirms this (Supplementary Fig. 8). Al_2O_3 with mainly Lewis sites did not convert **6** under identical reaction conditions. This further supports the conclusion that strong Brønsted acid sites in H-MOR are the active centers for aryl–alkyl cleavage. Notably, the conversion of **6** on Pt/H-MOR under a H_2 pressure of 40 bar

https://doi.org/10.1038/s44286-023-00006-0

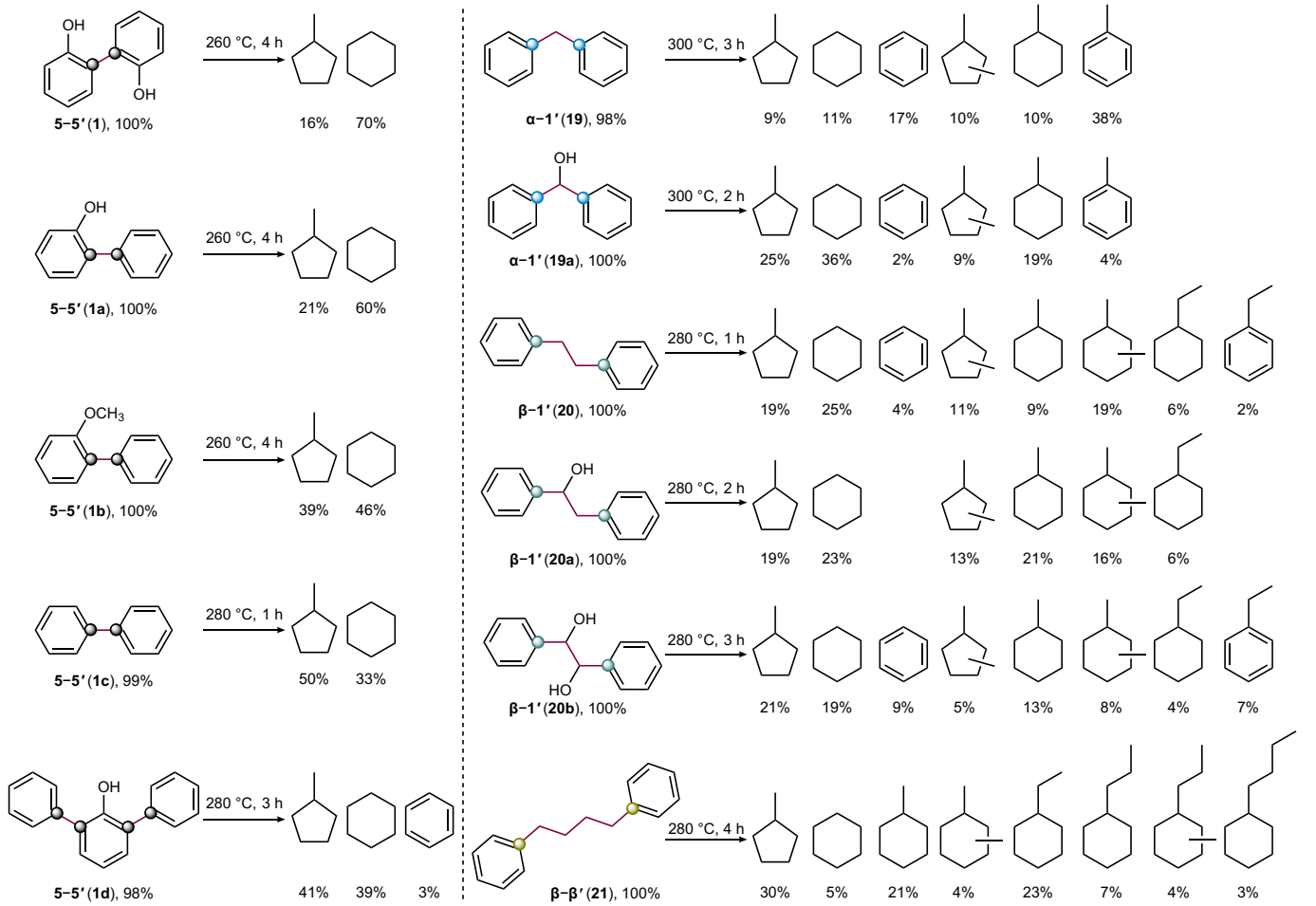

Fig. 4 | Substrate scope for reductive C–C cleavage. The numbers below each substrate and product refer to the conversion and yield, respectively. Detailed calculations of these parameters are provided in the Supplementary Information. Reaction conditions: substrate (20 mmol l^{-1}), 50 mg Pt/H-MOR, 40 ml of *n*-pentane and 40 bar H_2.

(Supplementary Fig. 7b) led to the formation of similar products. However, products **16** and **17** were not observed, presumably because they were rapidly hydrogenated. The reaction rate of 51.1 mmol l^{-1} h^{-1} obtained with Pt/H-MOR was more than five times higher than with H-MOR. This difference is a strong indication that, although direct cracking of **6** on strong acid sites is possible, the bifunctional conversion of **6** via phenylcyclohexene is much faster. From the model compound studies, we can infer that **1** is mainly converted through hydrocracking of **6** with a small contribution of cracking via **10**. This is further supported by the nearly similar yields of **13** and **14** during the conversion of **1** and **6**, while the conversion of **10** also led to heavier products.

To gain a molecular-level understanding of the C–C bond cleavage mechanism over zeolitic Brønsted acid sites, we performed density functional theory (DFT) calculations. To facilitate such calculations for zeolite, we employed an H-FAU zeolite model (Supplementary Fig. 9) instead of H-MOR. Compared with the more complex MOR topology, the faujasite zeolite topology comprises a network of uniform supercages with only one crystallographically distinct T site. Catalytic experiments showed that H-MOR and H-FAU display comparable catalytic behavior (Supplementary Table 5). Various reaction pathways were explored for the cracking of the C–C bond in **12** (1-cyclohexylcyclohexene, $C_6C_6^=$) (Fig. 3), which was observed as an intermediate in the cracking of **10**. The activation of $C_6C_6^=$ over zeolite Brønsted acid sites (Zeo–H^+) occurs via protonation of the C–C double bond, which proceeds either via transition state 1 (TS1) to a tertiary carbenium ion ($C_6C_6^{tert}$) or via TS2 to a secondary carbenium ion ($C_6C_6^{sec}$). As expected, forming a tertiary carbenium ion requires a lower reaction barrier ($\Delta E^{\neq}$ = 32 kJ mol^{-1}) than that of a secondary carbenium ion ($\Delta E^{\neq}$ = 72 kJ mol^{-1}). The conversion of $C_6C_6^{tert}$ to $C_6C_6^{sec}$ can be achieved by a 1,2-H shift (TS3, $\Delta E^{\neq}$ = 61 kJ mol^{-1}), which is followed by C–C bond cleavage to form the C_6 products **13** and **14**. The cracking of the $C_6C_6^{sec}$ carbenium occurs via β-scission (TS4, $\Delta E^{\neq}$ = 117 kJ mol^{-1}), which yields a secondary C_6 carbenium along with cyclohexene (C_6^{sec}/$C_6^=$). C_6^{sec} can deprotonate to another cyclohexene molecule or isomerize to a branched 5-ring structure ($CH_3C_5^{tert}$). The isomerization of C_6^{sec} to $CH_3C_5^{tert}$ occurs in two steps, in which C_6^{sec} is first rearranged to $CH_3C_5^{sec}$ and then to $CH_3C_5^{tert}$ via a 1,2-H shift with respective activation barriers of 52 and 33 kJ mol^{-1} (Supplementary Fig. 10). The deprotonation of C_6^{sec} and $CH_3C_5^{tert}$ yields cyclic alkenes, which will be hydrogenated to cyclohexane and methylcyclopentane in the presence of a hydrogenation function such as Pt[36]. As cyclohexane and methylcyclopentane were observed as the main products during the conversion of **10**, it is reasonable to conclude that C–C bond cleavage can also occur via intermediates with a cyclohexyl–methylene–cyclopentane skeleton. DFT calculations indicate that forming such intermediates (for example, $C_6CH^+C_5$) is facile via isomerization of $C_6C_6^{sec}$ with a relatively low barrier (TS5, $\Delta E^{\neq}$ = 27 kJ mol^{-1}). To obtain two cyclic compounds via β-scission, the $C_6CH^+C_5$ intermediate should be converted to a carbenium ion with the positive carbon center either in the 5-ring or the 6-ring ($C_6CH_2C_5^{tert}$, $C_6CH_2C_5^{sec}$, $C_6^{tert}CH_2C_5$ and $C_6^{sec}CH_2C_5$). The formation and interconversion of these carbenium ions can be achieved by intramolecular

https://doi.org/10.1038/s44286-023-00006-0

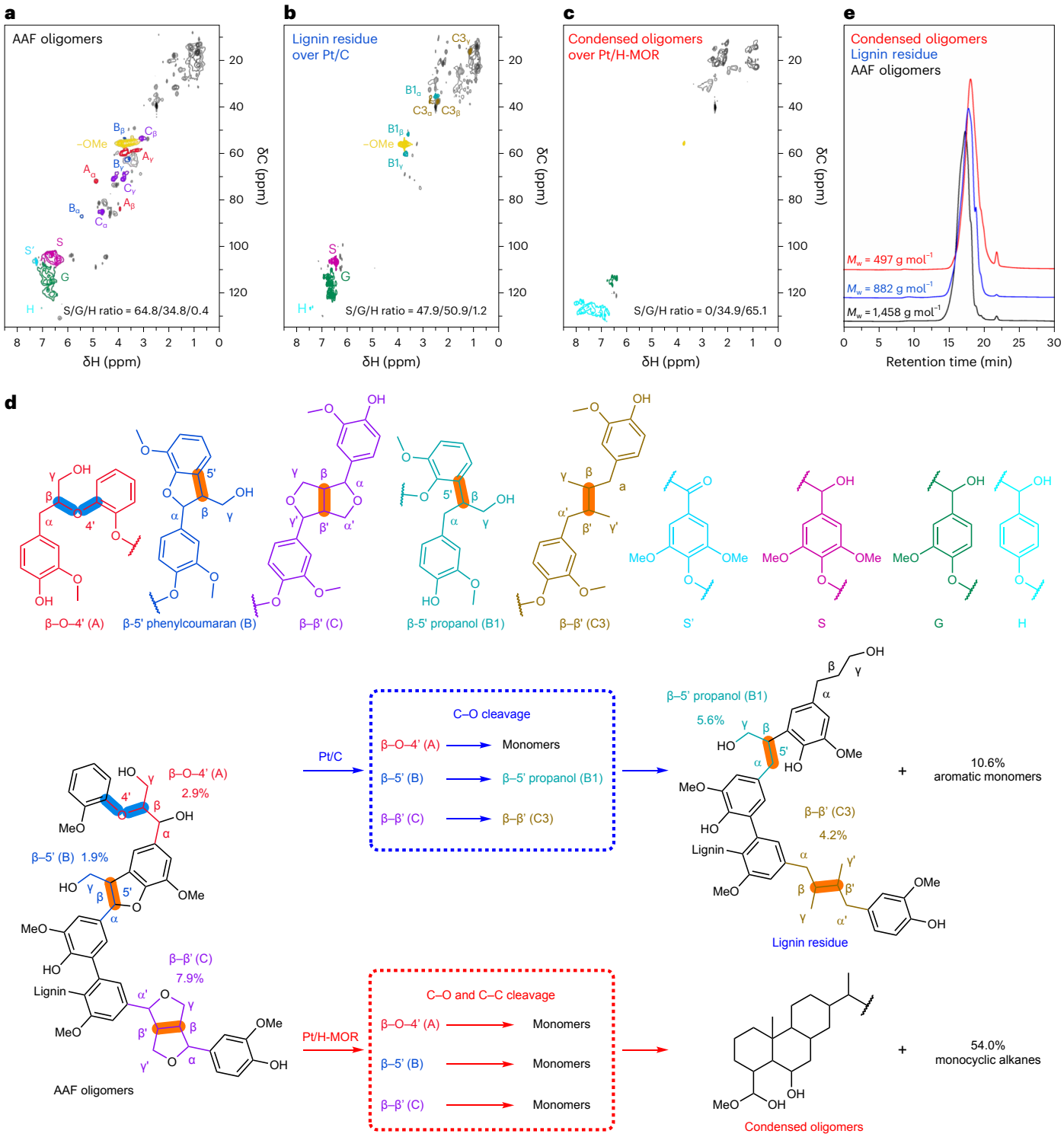

Fig. 5 | Reductive cleavage of AAF oligomers. a–c, 2D HSQC NMR spectra of AAF oligomers (**a**), lignin oil after hydrogenolysis of AAF oligomers over Pt/C (**b**) and lignin oil after hydrocracking of AAF oligomers over Pt/H-MOR (**c**). Reaction conditions: AAF oligomers (1.0 g), 500 mg 1 wt% Pt/H-MOR or 100 mg commercial 5 wt% Pt/C, 40 ml of *n*-pentane, 300 °C, 40 bar H_2 and 24 h. **d**, Hydrogenolysis of AAF oligomers over Pt/C resulted in a monomer yield of 10.6% via C–O cleavage. A substantially improved monomer yield of 54.0% over Pt/H-MOR was achieved via reductive C–C and C–O cleavage developed using Pt/H-MOR. **e**, GPC of AAF oligomers (black line), lignin oil obtained after hydrogenolysis of AAF oligomers over Pt/C (blue) and lignin oil obtained after hydrocracking of AAF oligomers over Pt/H-MOR (red).

H shifts with activation barriers in the range of 3–58 kJ mol^{-1} (Supplementary Fig. 11). Depending on the location of the positive carbon center, β-scission of $C_6CH^+C_5$-derived carbenium ions (TS6–9) leads to different combinations of cyclic reaction products (Supplementary Fig. 12). A comparison of the energy profiles indicates that these C–C bond cleavage pathways may provide an alternative to β-scission from $C_6C_6^{sec}$, although the latter route remains the most favorable (Fig. 3 and Supplementary Table 6).

Additional DFT calculations (Supplementary Note 3) demonstrate that a reaction pathway for the C–C cracking of phenylcyclohexene has a low barrier of 86 kJ mol^{-1}, which compares favorably with the barrier of 117 kJ mol^{-1} for cyclohexylcyclohexene. This explains the preference for C–C cleavage in **6** over **10**. Moreover, the direct C–C bond cleavage in phenylcyclohexane is also possible with a barrier of 134 kJ mol^{-1}. These results can explain the experimental finding that, although monomer formation from **6** is possible with H-MOR, the rate with Pt/H-MOR is much higher.

Based on this comprehensive understanding of C–C cleavage, we explored different substrates (Fig. 4). Biphenols substituted at the 2-2′-positions were evaluated at a reaction temperature of 260 °C. It is encouraging that different 2,2′-substituents (**1a** and **1b**) also led to monocyclic products in good yields. A substrate without hydroxyls (**1c**) required a higher reaction temperature (280 °C) to achieve a decent conversion to monocyclic products. Besides biphenol compounds with 5–5′ bonds, compounds with β–1′ linkages with hydroxyls placed at different positions at the carbon bridge were also evaluated. Conversion of such β–1′ linkages (**20**, **20a** and **20b**) required a temperature of 280 °C. The lower reactivity of such compounds compared to **1a**, **1b** and **1c** indicates that oxygen-containing substituents on the aromatic ring facilitate hydrogenation and subsequent aryl–alkyl cleavage. In addition to β–1′, bicyclic model compounds with methylene linkages (**19** and **19a**) representing α–1′ bonds were converted. Such bonds are typically found in technical lignins due to self-condensation or formaldehyde-induced condensation of lignin fragments during acidic and alkaline fractionation[37,38]. Compared with 5–5′ and β–1′ bonds, achieving a high yield of monocyclic products by cleavage of the α–1′ bonds in **19** and **19a** demanded a higher reaction temperature of 300 °C. The increase in the temperature required to selectively cleave 5–5′, β–1′ and α–1′ bonds did not correlate with their bond dissociation energies, suggesting that C–C cleavage was also affected by other aspects such as the presence of hydroxyl groups on the aromatic ring in the β–1′ linkage. 1,4-Diphenylbutane (**21**), employed to represent the β–β′ linkage, could be converted to monocyclic hydrocarbons with a yield of 98%. It was also found that a bulkier trimer compound (5–5′ trimer, **1d**) could be decomposed into monocyclic compounds with a high yield at a temperature of 280 °C, further confirming the promise of our approach.

With a reliable approach for selectively cleaving C–C bonds in hand, we were motivated to examine the potential of depolymerizing oligomers obtained by aldehyde-assisted fractionation (AAF oligomers; Extended Data Table 1 and Fig. 5). The feedstock was obtained by fractionation of hardwood using isobutyraldehyde as a capping agent to hinder recondensation, followed by catalytic hydrogenolysis of the isolated lignin[39]. The depolymerization of these AAF oligomers over Pt/H-MOR yielded 54.0% monocyclics at 300 °C (Extended Data Table 1 and Supplementary Table 7). For comparison, hydrogenolysis with Pt/C as a catalyst and oxidation with alkaline nitrobenzene oxidation (NBO) gave respective monomer yields of 10.6% (Extended Data Table 1 and Supplementary Table 8) and 9.5% (Extended Data Table 1 and Supplementary Table 9), suggesting that the monomer yield related to C–O bond cleavage was ~10%. Thus, the fivefold increase to 54.0% in monomer yield over Pt/H-MOR results from C–C bond cleavage, in line with the predominance of such linkages in the AAF oligomers (Fig. 5a and Supplementary Table 10). C–C bond cleavage was confirmed by observing partially hydrogenated bicyclic compounds after 1 h and their cleavage to monomers after 4 h (Supplementary Figs. 13 and 14). Whereas five different dimeric compounds containing β–β′, 5–5′, α–1′, β–5′ and β–1′ linkages were observed in the lignin oil obtained with Pt/C (Supplementary Fig. 15), these compounds were absent with Pt/H-MOR as the catalyst (Supplementary Fig. 16). The occurrence of C–C cleavage was further supported by a comparison of $^{1}H/^{13}C$ 2D heteronuclear single quantum coherence (HSQC) spectra of the AAF oligomers (Fig. 5a) and the lignin oils extracted upon conversion with Pt/C (Fig. 5b) and Pt/H-MOR (Fig. 5c). The AAF oligomers were composed of S (syringyl)-derived phenylpropanol, G (guaiacyl) and H (p-hydroxylphenyl) building blocks with an S/G/H ratio of 64.8/34.8/0.4, which are connected by β–O–4′ (A), β–5′ (B) and β–β′ (C) linkages. After depolymerization, the β–5′ (B1) and β–β′ (C3) linkages remained intact, with Pt/C (Fig. 5b,d) accounting for 9.8% of the C_9 units in the reacted lignin, similar to the content in the parent lignin. In contrast, β–5′ and β–β′ bonds were completely cleaved with Pt/H-MOR (Fig. 5c,d). Correspondingly, the H content of the lignin oil obtained with Pt/C slightly increased to 1.2% (S/G/H = 47.9/50.9/1.2), which was accompanied by a decrease in the number of methoxy groups. The increase in the H content to 65.1% (0/34.9/65.1) with Pt/H-MOR can be explained by the high deoxygenation activity of our catalyst. The use of the bifunctional Pt/H-MOR catalyst led to a significant reduction of the molecular weight (M_w) of the condensed oligomers to 497 g mol^{-1}, in comparison with the value of 882 g mol^{-1} for the lignin residue obtained with Pt/C, as determined by gel permeation chromatography (GPC; Fig. 5e). The Pt/H-MOR catalyst could be reused at least four times without any loss of activity in the conversion of AAF oligomers (Supplementary Note 4). The utility of our approach was further assessed in the upgrading of lignin oligomers obtained by the RCF of birchwood. The RCF step yielded a lignin oil containing 42.3% monomers. Further conversion of the lignin oil over Pt/H-MOR increased the total monomer yield to 76.9%, representing a nearly twofold increase over the theoretical maximum monomer yield (Supplementary Note 5).

The broader utility of our approach towards technical lignin was established for a range of lignins fractionated from hardwood and softwood using methods such as acid methanolysis (methanolysis lignin), sulfite pulping (Kraft lignin), alkaline pulping (soda lignin), alkaline pulping with methanolysis (soda-methanolysis lignin), supercritical water extraction (water-extracted lignin) and acid hydrolysis with enzymolysis (enzymatic-hydrolysis lignin) (detailed information is provided in Supplementary Tables 10–13). In all cases, this approach led to a significant improvement of the monomer yield (Extended Data Table 1), that is, by 16.8% for the methanolysis lignin (Supplementary Fig. 17), 6.0% for the Kraft lignin (Supplementary Fig. 18), 12.0% for the soda lignin (Supplementary Fig. 19), 12.4% for the soda-methanolysis lignin (Supplementary Fig. 20), 8.6% for the water-extracted lignin (Supplementary Fig. 21) and 7.9% for the enzymatic-hydrolysis lignin (Supplementary Fig. 22), referenced to values obtained by NBO and Pt/C hydrogenolysis. The HSQC and GPC results (Fig. 5 and Supplementary Figs. 17–22) showed that the β–5′ and β–β′ linkages in the seven lignins were completely cleaved during their conversion with the Pt/H-MOR catalyst, while most remained intact with Pt/C. This difference illustrates that the type of C–C linkage did not significantly affect the monomer yield achieved by our approach. Among the significant improvements in monomer yield, the extent of C–C cleavage was highest for the AAF oligomers. Comparison of typical properties that can serve as indicators to predict the monomer yield, such as β–O–4′ content[12] (Supplementary Fig. 23a), S/G ratio[40] (Supplementary Fig. 23b) and molecular weight[41] (Supplementary Fig. 23c), did not provide a satisfactory explanation for the outstanding results obtained with the AAF oligomers. Instead, we speculate that the H content plays an important role (Supplementary Fig. 23d). Although the water-extracted lignin has a higher H content than the AAF oligomers, it is poorly soluble in various apolar solvents, which can explain the poor C–C cleavage performance in our approach. The substrate scope study showed that cleaving the C–C bond in the compound representing H units (**1** in Fig. 4) is much easier than others. This aspect can be further utilized in future studies by employing a larger population of natural variants to perform multivariate studies[42].

We then designed a process involving our C–C bond cleavage approach (Fig. 6a, Supplementary Fig. 24 and Supplementary Table 14) to perform a techno-economic analysis (TEA) and a life-cycle assessment (LCA) for a biorefinery based on AAF oligomers. The process

https://doi.org/10.1038/s44286-023-00006-0

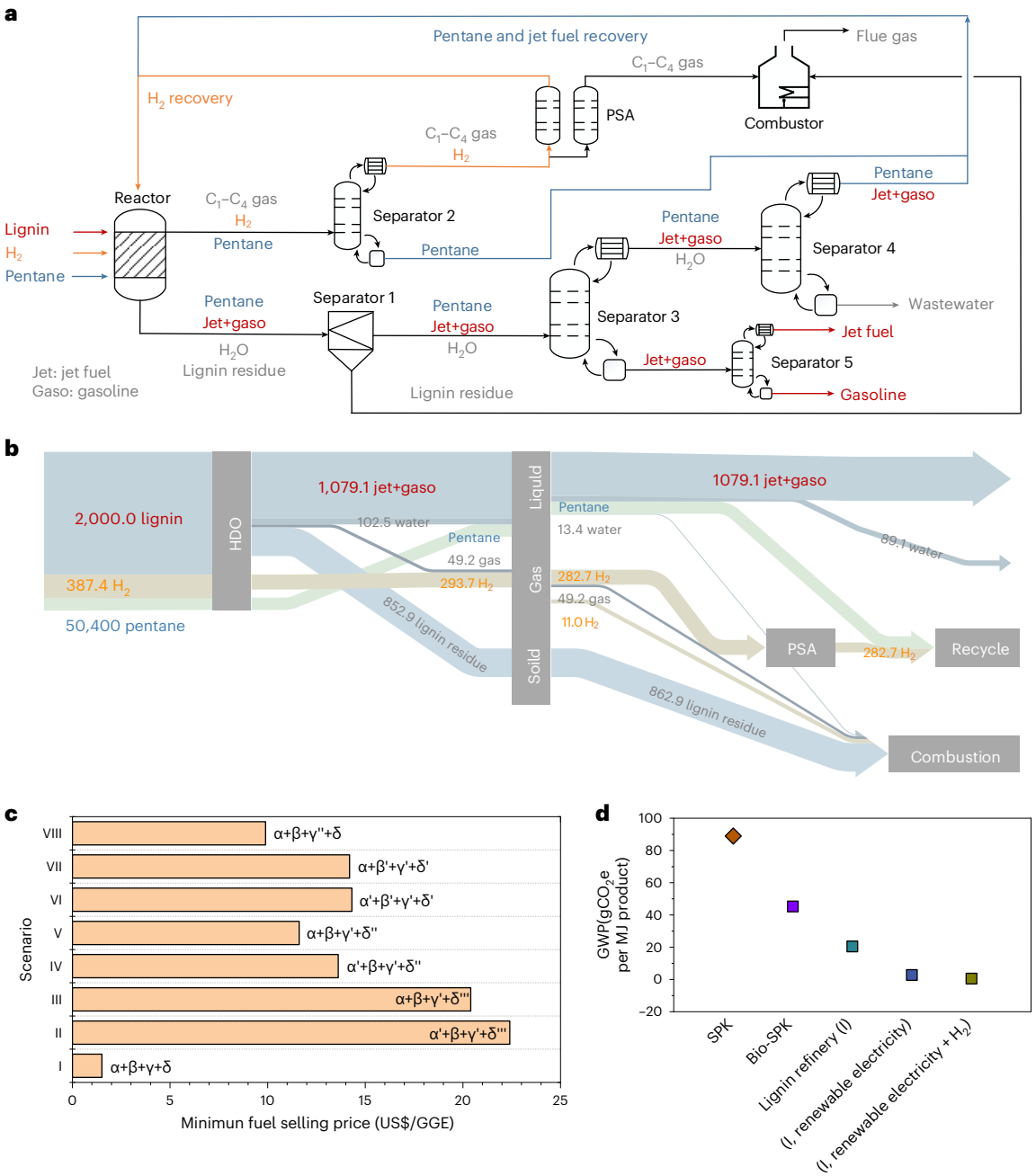

Fig. 6 | Process layout and details of the proposed AAF oligomers refinery. **a**, Proposed block flow diagram to produce jet fuel and gasoline components from the reductive cleavage of C–C bonds in lignin. **b**, Mass flows (t d^{-1}) of the lignin biorefinery. **c**, Minimum jet fuel selling price (MFSP) for various scenarios based on a West Texas Intermediate (WTI) price of US$96.5 per barrel and a gasoline price of US$1,161.1 per ton. H_2 consumption is based on the oxygen content in the model compound (β–O–4′, α) and lignin (elemental analysis, α′); H_2 recycle: Yes (β) and No (β′); combustion of lignin (γ), pentane (γ′), and gasoline and lignin (γ′); solvent loss at 0.2% (δ), 1% (δ′), 3% (δ′) and 5% (δ″). **d**, Global warming potential (GWP) (gCO_2e per MJ product) of biofuel in different scenarios.

involves the complete hydrodeoxygenation (HDO) of the intermediates obtained by the C–C bond cleavage strategy. The product consists of alkylated cyclohexanes and monoaromatics with a gasoline-range C_6–C_8 fraction (74.9%) and a fraction of C_9–C_{10} compounds (25.1%), which can be blended with (renewable) jet fuel (Supplementary Table 15). Renewable jet fuel can be derived from various sources, such as synthetic paraffinic kerosene (SPK) obtained by Fischer–Tropsch synthesis[43], biomass-derived synthetic paraffinic kerosene (Bio-SPK)[44] and hydroprocessed esters and fatty acids (HEFA)[45] from animal fats and plant oils, which mainly consist of *n*- and *iso*-alkanes. According to ASTM D7566-14a[46], jet fuel should contain at least 8 vol% of aromatics and up to 15 vol% of cycloalkanes, which can be obtained from the proposed catalytic process by liquid–solid separation (separator 1) and liquid fractionation (separators 3 and 5). The water formed during lignin HDO ends up in the wastewater stream from separator 4. The gaseous mixture comprising C_1–C_4 gases, *n*-pentane and H_2 is fed to the condenser (separator 2), in which *n*-pentane, together with the collected *n*-pentane and biofuel from separator 4, is recycled back to the reactor. The remaining gas mixture of C_1–C_4 hydrocarbons and H_2 is processed in the pressure swing adsorption (PSA) section, separating the C_1–C_4 components from H_2, the latter being recycled to the reactor. The C_1–C_4 gas and the lignin residue from separator 1 are combusted for

heat recovery. The mass flows in Fig. 6b (also Supplementary Tables 16 and 17) show that the conversion of 2,000 tons of AAF oligomers yields 270.1 tons of jet fuel and 809.0 tons of gasoline, corresponding to 54 wt% of the lignin intake. The HDO process consumes 24% of the H_2, while 2% of the H_2 is lost in the liquid–gas separation and PSA processes. Analysis of the carbon-based flows (Supplementary Fig. 25) reveals that 49.9% of lignin is converted to jet fuel-compatible mixtures, gasoline, lignin residue and gas with carbon yields of 21.1%, 63.3%, 12.9% and 2.8%, respectively. The remaining lignin (50.1%) was burned for energy. The energy flows (Supplementary Fig. 26 and Supplementary Table 18) demonstrate that operating the biorefinery necessitates the additional combustion of lignin to fulfill the remaining 39.4% of the energy requirement.

The TEA of the proposed biorefinery (Fig. 6c) was calculated for a daily treatment of 2,000 tons of lignin[41]. The combustor (32.7%) and high-pressure reactor (25.3%) were the most expensive pieces of equipment (Supplementary Fig. 27). Concerning operational expenditure, the feedstock was the most significant contributor to the manufacturing cost (Supplementary Fig. 28 and Supplementary Tables 19 and 20). Eight different scenarios (Supplementary Table 21) were compared, considering the mode of H_2 consumption, H_2 recycle, solvent loss and feedstock/product combustion on the operating cost. The minimum fuel selling price (MFSP) was determined using a 10% discount rate without considering taxation. The selling price of the product was adjusted to achieve a net present value (NPV) of zero. Based on the design and economic basis (Supplementary Table 22), scenario I reached the lowest MFSP of US$1.51 per gasoline gallon equivalent (GGE). This was mainly due to the higher yield of target products, such as gasoline, and the reduced solvent consumption through lignin combustion. Given the current pricing of jet fuel and gasoline, the optimized scenario I offers a rough internal rate of return of 23.0% and a payout time of 6.6 years for a plant with a lifetime of 20 years (Supplementary Table 23).

We also carried out an LCA of this process (Fig. 6d, Supplementary Fig. 29 and Supplementary Tables 24–27). Optimized scenario I was compared to standard scenarios, including SPK[43] and Bio-SPK[44]. As expected, scenario I showed the lowest greenhouse-gas emissions at 20.4 $gCO_2e\ MJ^{-1}$ jet fuel and gasoline, giving respective decreases of 55.0% and 77.1% compared to Bio-SPK and SPK. The greenhouse-gas emissions would decrease to 0.47 $gCO_2e\ MJ^{-1}$ jet fuel and gasoline using renewable electricity and H_2, unveiling the possibility for a CO_2-neutral lignin biorefinery aimed at fuel production.

Current biorefining efforts remain strongly hampered by the low value of lignin waste, even when part of the lignin can be valorized into valuable building blocks in the lignin-first approach. The present study demonstrates a technology to convert recalcitrant lignin sources rich in C–C bonds into valuable products for sustainable aviation purposes, contributing to reducing the carbon footprint of this hard-to-abate sector in terms of greenhouse-gas emissions. The developed catalytic approach selectively disrupts various C–C linkages without pre-functionalization under relatively mild conditions. It is based on the synergistic action between a Pt (de)hydrogenation function and Brønsted acid sites confined in the micropores of zeolite. We have demonstrated that this hydrocracking strategy is effective for upgrading oligomers obtained by aldehyde-assisted fractionation or RCF from lignocellulosic biomass, as well as various technical lignins, underpinning the broad utility of our approach. As such, this technology can be easily integrated into different biorefining schemes, bringing the valorization of some 70 million tons of lignin waste annually produced closer to reality.

Methods

Preparation of catalysts

Pt was loaded on various support materials by wetness impregnation. In a typical synthesis, 1.0 g of H-MOR was suspended in a tetraammineplatinum(II) nitrate solution, prepared by dissolving 0.0198 g $(Pt(NH_3)_4(NO_3)_2$ in 20 ml of deionized water. After stirring for 2 h, the mixture was dried at 80 °C overnight. The powder was calcined in flowing artificial air at 300 °C for 4 h, followed by reduction in a 50 vol% H_2 in He flow at 300 °C for 4 h (1 °C min^{-1}). The Pt content of Pt/H-MOR was ~1 wt%. Na-exchanged H-MOR catalyst was prepared by three times ion exchange with a 1 M $NaNO_3$ solution at 40 °C for 24 h, followed by centrifugation and drying at 80 °C overnight. The Pt/Na-MOR zeolite was obtained in the same way as Pt/H-MOR. Pt was loaded on other support materials in the same way. Ru/H-MOR, Ni/H-MOR and Cu/H-MOR were obtained by incipient wetness impregnation using aqueous solutions of $RuCl_3$, $Ni(NO_3)_2{\cdot}6H_2O$ and $Cu_2(NO_3)_4{\cdot}5H_2O$, respectively, of appropriate concentration under vigorous stirring for 2 h. The resulting solid mixture was dried, calcined and reduced in the same way as the Pt-containing zeolites, except for the Ru/H-MOR zeolite, which was calcined in He.

Conversion of lignin model compounds and lignins

In lignin model compound conversion studies, the substrate (20 mmol l^{-1}) and catalyst (50 mg) were loaded into a 100-ml Parr reactor with *n*-pentane (40 ml) as the solvent. Once closed, the reactor was purged with N_2 five times and charged with H_2 at 40 bar. The reactor was heated to the desired temperature, followed by a dwell under stirring (650 r.p.m.). Liquid products for gas chromatography (GC) analysis were sampled during the experiment. After the reaction, the reactor was cooled in an ice bath until the temperature was below 10 °C, at which time the gaseous products were collected for GC analysis. In lignin conversion studies, 1.0 g of lignin powder was mixed with 500 mg of solid catalyst. The remaining procedure was the same as described above.

^1H–^{13}C HSQC NMR of lignin

Approximately 100 mg of dried lignin was dissolved in 0.7 ml of dimethylsulfoxide-d_6 (DMSO-d_6). NMR spectra were recorded using a VARIAN INOVA 500-MHz spectrometer equipped with a 5-mm ID Auto ID PFG probe (128 scans acquired from 0 to 16 ppm in the F2 (^1H) dimension with 1,200 data points (acquisition time 10 ms) and 44 scans with 0 to 200 ppm in the F1 (^{13}C) dimension with 256 t1 increments (acquisition time 10 ms) and 2-s relaxation time). Data were processed using MestreNova software. The DMSO solvent peak was used as an internal reference (δ_C = 39.5 ppm, δ_H = 2.50 ppm). Semi-quantitative analysis of the HSQC NMR spectra was done by integration of the correlation peaks in the different regions of the spectra according to literature methods[47]. The relative quantity of side chains involved in the inter-unit and terminal substructures is expressed as a number per 100 aromatic units (S + G).

Derivatization and analysis of dimers in lignin oils

Derivatization was performed as described previously[40]. Dried lignin oil samples were prepared for dissolving in dichloromethane to obtain a 10-mg-ml^{-1} solution. Six hundred microliters of 10-mg-ml^{-1} lignin oil solution were added to a 2-ml GC vial, followed by the addition of 50 µl of pyridine and 100 µl of silylating agent. N,O-bis(trimethylsilyl) trifluoroacetamide (BSTFA) with 1% trimethylchlorosilane was used as the silylating agent. As this compound reacts readily with water, BSTFA was applied immediately after opening the cap, followed by immediately closing the GC vial. The lignin oil, pyridine and BSTFA solution were then heated for 30 min at 50 °C before being injected on the GC-MS.

Computational methods

Periodic DFT calculations were performed using the Vienna Ab initio Simulation Package (VASP, version 5.4.4). The Perdew–Burke–Ernzerhof (PBE) functional was combined with the projector augmented wave (PAW) method. The cutoff energy of the plane-wave basis sets

was set to 500 eV. The Brillouin zone sampling was restricted to the Γ point. Van der Waals interactions were described by the DFT-D3 (BJ) method. Structures were assumed to be converged when the force on each atom was below 0.05 eV $Å^{-1}$. The minimum-energy reaction paths and corresponding transition states were determined by the climbing image nudged elastic band (CI-NEB) method. The maximum energy geometries along the reaction path from CI-NEB calculations were further optimized using a quasi-Newton algorithm. FAU zeolite was simulated using a rhombohedral 48 T unit cell ($Si_{48}O_{96}$). Brønsted acid sites were introduced by replacing one of the lattice Si with an Al atom with a charge-compensating proton (H^+) being added to the anionic oxygen site (Supplementary Fig. 9). The cell parameters were first optimized, followed by complete geometry optimization with guest molecules with fixed lattice parameters ($a = b = c = 17.29$ Å, $\alpha = \beta = \gamma = 60°$).

Process design details for TEA and LCA

The process simulations were performed using Aspen Plus (V10.0). ENVIRON was used as a method filter, and METCBAR was chosen as the global unit. For modeling the equilibrium data of jet fuel and gasoline, the Soave–Redlich–Kwong equation of state (SRK) method is used. Details on the assumptions for these process simulations and input data are described in the Supplementary Information. Briefly, the reactors were operated in a steady state, assuming uniform temperatures and pressures in the reactors. The units were designed to process 2,000 tons of lignin per day. The reaction conditions for the hydrotreatment step were 300 °C, 4 MPa and a reaction time of 24 h. The lignin/*n*-pentane/hydrogen mass ratio was 1/25.2/0.19. The stripping conditions used for gas–liquid separations were 25 °C and 3 bar. The stripping conditions for the liquid–liquid separation were 40 °C and a vapor fraction of 0.9. The jet fuel and gasoline/water mass ratio during separation is 1/0.095. The combustion of C_1–C_4 gas, H_2 and lignin residues was carried out at 900 °C and 1 bar. In the system, excess heat is used to produce steam as a by-product. Moreover, gaseous products (C_1–C_4 gas and a small amount of hydrogen) and lignin residues are fed into the combustion chamber to supply heat.

Methodology for TEA

TEA includes a detailed process flow diagram (based on research data), rigorous materials and energy balance calculations (via Aspen Plus simulation tools), capital and project cost estimation (percentages of the total equipment costs and revenues[14]), and calculations of a net present value of zero (NPV) and a minimum fuel selling price. The project length is 20 years. The operation time is 7,884 h per year. The total plant cost includes equipment cost, other direct costs (installation, building and auxiliaries) and indirect costs (engineering and contingency). Direct costs are specified as 50% of equipment cost. Indirect costs are calculated to be 30% of equipment cost and direct costs. The monetary price of the products and raw materials is considered as the average market price in 2020. The lifetime of the Pt/H-MOR catalyst was assumed to be one year.

Methodology for LCA

The system boundaries encompass a cradle-to-gate approach (Supplementary Fig. 29), meaning that the analysis considers all stages in the life-cycle of the products. These stages include hydrogenolysis of the isolated lignin obtained during fractionation of hardwood using isobutyraldehyde protection, transportation of AAF1 oligomers, and the production of jet fuel and gasoline. The first two processes do not consider CO_2 emissions, because AAF1 oligomers are considered a by-product. The production of jet fuel and gasoline (Supplementary Fig. 24 and Fig. 6a) includes hydrotreatment, liquid–solid separation, liquid–liquid fractionation, hydrogen pressure swing adsorption (PSA), liquid and gas circulation, and combustion. The input is composed of catalyst, hydrogen, pentane and electricity. The CO_2 emissions for the usage of jet fuel and gasoline are not included due to the carbon-neutral property of AAF1 oligomers.

The GWP was studied using SimaPro software (9.4.0.1). The Ecoinvent 3 and Industry data 2.0 LCI databases were used to determine the environmental impact of the existing technologies and production processes. 'Cut-off, S' is selected as the model to analyze the GWP of the feedstock. The data in the process are determined from laboratory experiments, which are simulated on an industrial scale accompanied by the TEA. The allocation of CO_2 emission is based on the economic value of the products. The assessment method used was IPCC 2013 GWP 100a.

Data availability

All data are available within the manuscript and Supplementary Information. The atomic coordinates of the optimized computational models are provided in Supplementary Data 1. Source data are provided with this paper.

References

1. Questell-Santiago, Y. M., Galkin, M. V., Barta, K. & Luterbacher, J. S. Stabilization strategies in biomass depolymerization using chemical functionalization. *Nat. Rev. Chem.* **4**, 311–330 (2020).
2. Liao, Y. et al. A sustainable wood biorefinery for low-carbon footprint chemicals production. *Science* **367**, 1385–1390 (2020).
3. Li, C., Zhao, X., Wang, A., Huber, G. W. & Zhang, T. Catalytic transformation of lignin for chemicals and fuels. *Chem. Rev.* **115**, 11559–11624 (2015).
4. Sun, Z. et al. Complete lignocellulose conversion with integrated catalyst recycling yielding valuable aromatics and fuels. *Nat. Catal.* **1**, 82–92 (2018).
5. Tuck, C. O., Pérez, E., Horváth, I. T., Sheldon, R. A. & Poliakoff, M. Valorization of biomass: deriving more value from waste. *Science* **337**, 695–699 (2012).
6. Ragauskas, A. J. et al. Lignin valorization: improving lignin processing in the biorefinery. *Science* **344**, 1246843 (2014).
7. Rahimi, A., Ulbrich, A., Coon, J. J. & Stahl, S. S. Formic-acid-induced depolymerization of oxidized lignin to aromatics. *Nature* **515**, 249–252 (2014).
8. Li, Y. et al. An 'ideal lignin' facilitates full biomass utilization. *Sci. Adv.* **4**, eaau2968 (2018).
9. Meng, Q. et al. Sustainable production of benzene from lignin. *Nat. Commun.* **12**, 4534 (2021).
10. Katahira, R., Elder, T. J. & Beckham, G. T. in *A Brief Introduction to Lignin Structure*. (ed Beckham, G. T.) Ch. 1 (Royal Society of Chemistry, 2018).
11. Zakzeski, J., Bruijnincx, P. C., Jongerius, A. L. & Weckhuysen, B. M. The catalytic valorization of lignin for the production of renewable chemicals. *Chem. Rev.* **110**, 3552–3599 (2010).
12. Phongpreecha, T. et al. Predicting lignin depolymerization yields from quantifiable properties using fractionated biorefinery lignins. *Green Chem.* **19**, 5131–5143 (2017).
13. Talebi Amiri, M., Dick, G. R., Questell-Santiago, Y. M. & Luterbacher, J. S. Fractionation of lignocellulosic biomass to produce uncondensed aldehyde-stabilized lignin. *Nat. Protoc.* **14**, 921–954 (2019).
14. Biermann, C. J. *Handbook of Pulping and Papermaking* (Elsevier, 1996).
15. da Costa Sousa, L. et al. Next-generation ammonia pretreatment enhances cellulosic biofuel production. *Energy Environ. Sci.* **9**, 1215–1223 (2016).
16. Kim, K. H. et al. Integration of renewable deep eutectic solvents with engineered biomass to achieve a closed-loop biorefinery. *Proc. Natl Acad. Sci. USA* **116**, 13816–13824 (2019).
17. Luterbacher, J. S. et al. Nonenzymatic sugar production from biomass using biomass-derived γ-valerolactone. *Science* **343**, 277–280 (2014).

18. Feghali, E., Carrot, G., Thuery, P., Genre, C. & Cantat, T. Convergent reductive depolymerization of wood lignin to isolated phenol derivatives by metal-free catalytic hydrosilylation. *Energy Environ. Sci.* **8**, 2734–2743 (2015).
19. Deuss, P. J. et al. Phenolic acetals from lignins of varying compositions via iron (III) triflate catalysed depolymerisation. *Green Chem.* **19**, 2774–2782 (2017).
20. Renders, T. et al. Lignin-first biomass fractionation: the advent of active stabilisation strategies. *Energy Environ. Sci.* **10**, 1551–1557 (2017).
21. Wu, X. et al. Solar energy-driven lignin-first approach to full utilization of lignocellulosic biomass under mild conditions. *Nat. Catal.* **1**, 772–780 (2018).
22. Schutyser, W. et al. Chemicals from lignin: an interplay of lignocellulose fractionation, depolymerisation and upgrading. *Chem. Soc. Rev.* **47**, 852–908 (2018).
23. Rinaldi, R. et al. Paving the way for lignin valorisation: recent advances in bioengineering, biorefining and catalysis. *Angew. Chem. Int. Ed.* **55**, 8164–8215 (2016).
24. Kim, S. et al. Computational study of bond dissociation enthalpies for a large range of native and modified lignins. *J. Phys. Chem. Lett.* **2**, 2846–2852 (2011).
25. Subbotina, E. et al. Oxidative cleavage of C–C bonds in lignin. *Nat. Chem.* **13**, 1118–1125 (2021).
26. Hemberger, P., Custodis, V. B., Bodi, A., Gerber, T. & van Bokhoven, J. A. Understanding the mechanism of catalytic fast pyrolysis by unveiling reactive intermediates in heterogeneous catalysis. *Nat. Commun.* **8**, 15946 (2017).
27. Shuai, L. et al. Selective C-C bond cleavage of methylene-linked lignin models and kraft lignin. *ACS Catal.* **8**, 6507–6512 (2018).
28. Zhu, J., Wang, J. & Dong, G. Catalytic activation of unstrained C(aryl)–C(aryl) bonds in 2,2′-biphenols. *Nat. Chem.* **11**, 45–51 (2019).
29. Zhu, J., Xue, Y., Zhang, R., Ratchford, B. & Dong, G. Catalytic activation of unstrained C(aryl)–C(alkyl) bonds in 2,2′ -methylenediphenols. *J. Am. Chem. Soc.* **144**, 3242–3249 (2022).
30. Wang, W. et al. Microwave-assisted catalytic cleavage of C–C bond in lignin models by bifunctional Pt/CDC-SiC. *ACS Sustain. Chem. Eng.* **8**, 38–43 (2019).
31. Li, X. et al. Scission of C–O and C–C linkages in lignin over RuRe alloy catalyst. *J. Energy Chem.* **67**, 492–499 (2022).
32. Dong, L. et al. Breaking the limit of lignin monomer production via cleavage of interunit carbon–carbon linkages. *Chem* **5**, 1521–1536 (2019).
33. Luo, Z. et al. Hydrothermally stable Ru/HZSM-5-catalyzed selective hydrogenolysis of lignin-derived substituted phenols to bio-arenes in water. *Green Chem.* **18**, 5845–5858 (2016).
34. Weitkamp, J. Catalytic hydrocracking—mechanisms and versatility of the process. *ChemCatChem* **4**, 292–306 (2012).
35. Mirena, J. I. et al. Impact of the spatial distribution of active material on bifunctional hydrocracking. *Ind. Eng. Chem. Res.* **60**, 6357–6378 (2021).
36. Chen, G. et al. Interfacial electronic effects control the reaction selectivity of platinum catalysts. *Nat. Mater.* **15**, 564–569 (2016).
37. Huang, X., Korányi, T. I., Boot, M. D. & Hensen, E. J. Ethanol as capping agent and formaldehyde scavenger for efficient depolymerization of lignin to aromatics. *Green Chem.* **17**, 4941–4950 (2015).
38. Sturgeon, M. R. et al. A mechanistic investigation of acid-catalyzed cleavage of aryl-ether linkages: implications for lignin depolymerization in acidic environments. *ACS Sustain. Chem. Eng.* **2**, 472–485 (2014).
39. Shuai, L. et al. Formaldehyde stabilization facilitates lignin monomer production during biomass depolymerization. *Science* **354**, 329–333 (2016).
40. Anderson, E. M. et al. Differences in S/G ratio in natural poplar variants do not predict catalytic depolymerization monomer yields. *Nat. Commun.* **10**, 2033 (2019).
41. Humbird, D. et al. *Process Design and Economics for Biochemical Conversion of Lignocellulosic Biomass to Ethanol: Dilute-Acid Pretreatment and Enzymatic Hydrolysis of Corn Stover* (National Renewable Energy Laboratory, 2011); https://www.nrel.gov/docs/fy11osti/47764.pdf
42. Zhang, C. & Wang, F. Catalytic lignin depolymerization to aromatic chemicals. *Acc. Chem. Res.* **53**, 470–484 (2020).
43. Moses, C. A. Comparative evaluation of semi-synthetic jet fuels. *Contract* **33415**, 2299 (2008).
44. Rahmes, T., Kinder, J. & Crenfeldt, G. Sustainable bio-derived synthetic paraffinic kerosene (Bio-SPK) jet fuel flights and engine tests program results. In *Proc. 9th AIAA Aviation Technology, Integration and Operations Conference* (*ATIO*) *and Aircraft Noise and Emissions Reduction Symposium* (*ANERS*) 7002 (AIAA, 2009).
45. Enright, C. Aviation fuel standard takes flight. *ASTM Stand. News* **39**, 5 (2011).
46. *Standard Specification for Aviation Turbine Fuel Containing Synthesized Hydrocarbons*. ASTM Standard D7566-14a (ASTM international, 2014).
47. Zijlstra, D. S. et al. Extraction of lignin with high β-O-4 content by mild ethanol extraction and its effect on the depolymerization yield. *J. Vis. Exp* **143**, 58575 (2019).

Acknowledgements

This research was supported financially by the Chemelot Institute for Science and Technology awarded to E.J.M.H. Z.L. acknowledges support for the RCF experiments, TEA and LCA calculations from the National Natural Science Foundation of China (grant no. 52206236), the Natural Science Foundation of Jiangsu Province (grant no. BK20220837) and the Fundamental Research Funds for the Central Universities (3203002211A1). J.T.B.d.B. and J.S.L. were supported by the Swiss National Science Foundation through the National Competence Center Catalysis (grant no. 51NF40_180544). The contribution of A.R. was supported by the European Union's Horizon 2020 research and innovation programme under grant agreement no. 883753 (IDEALFUEL).

Author contributions

Z.L. and E.J.M.H. conceived the idea for lignin depolymerization. Z.L. and A.R. performed the reactions of lignin and lignin model compounds. C.L. conducted the DFT calculations. Y.W. and J.X. carried out the TEA and LCA calculations with guidance from H.Z. and R.X. P.D.K., M.D.B. and J.T.B.d.B., supervised by J.S.L., prepared the technical lignins. Z.L. and E.H. wrote the manuscript in close consultation with M.D.B., D.F.d.W., C.L., H.Z. and R.X. All authors contributed to the manuscript.

Competing interests

The authors declare no competing interests.

Additional information

Extended data is available for this paper at https://doi.org/10.1038/s44286-023-00006-0.

Supplementary information The online version contains supplementary material available at https://doi.org/10.1038/s44286-023-00006-0.

Correspondence and requests for materials should be addressed to Zhicheng Luo, Rui Xiao or Emiel J. M. Hensen.

Peer review information *Nature Chemical Engineering* thanks Changzhi Li, Joseph Samec, Yanqin Wang and the other, anonymous, reviewer(s) for their contribution to the peer review of this work.

https://doi.org/10.1038/s44286-023-00006-0

Extended Data Table 1 | Monomers obtained from various technical lignins using different methods, including alkaline nitrobenzene oxidation (NBO), Pt/C-catalyzed hydrogenolysis, and Pt/H-MOR-catalyzed hydrocracking

Entry	Lignin source	Monomer yield (mol%)			
		C–O Cleavage		C–O and C–C cleavage	C–C cleavage[d]
		NBO[a]	Pt/C[b, e]	Pt/H-MOR[c, e]	
1	AAF oligomers	9.5	10.6	54.0	44.0
2	Methanolysis	3.3	5.5	21.2	16.8
3	Kraft	11.5	10.8	17.1	6.0
4	Soda	7.3	7.5	19.4	12.0
5	Soda	8.8	9.4	21.5	12.4
6	Water-extracted	7.9	8.6	16.8	8.6
7	Enzymatic-hydrolysis	3.7	4.9	12.2	7.9
8	Birch wood	-	42.3[f]	76.9	34.6

[a] Monomer obtained from alkaline nitrobenzene oxidation (NBO).
[b] Monomer obtained from hydrogenolysis over commercial Pt/C.
[c] Monomer obtained from hydrocracking over Pt/H-MOR.
[d] Improved monomer yield results from the C–C cleavage; defined as Pt/H-MOR – (NBO + Pt/C)/2.
[e] Reaction conditions: Lignin (1.0 g), 500 mg 1 wt% Pt/H-MOR or 100 mg commercial 5 wt% Pt/C, 40 mL n-pentane, 24 h, 300 °C, and 40 bar H_2.
[f] Conventional RCF process with the theoretical maximum monomer yield.

[a]Monomer obtained from alkaline nitrobenzene oxidation (NBO). [b]Monomer obtained from hydrogenolysis over commercial Pt/C. [c]Monomer obtained from hydrocracking over Pt/H-MOR. [d]Improved monomer yield results from the C–C cleavage; defined as Pt/H-MOR – (NBO + Pt/C)/2. [e]Reaction conditions: Lignin (1.0 g), 500 mg 1 wt% Pt/H-MOR or 100 mg commercial 5 wt% Pt/C, 40 mL n-pentane, 24 h, 300 °C, and 40 bar H2. [f]Conventional RCF process with the theoretical maximum monomer yield.